coatings

MDPI

Article

Effect of Cu and Ni Inclusion on Tribological Performance of Tribocatalytically Active Coatings in Hydrocarbon Environments

Rawan Al Sulaimi, Mohammad Eskandari, Asghar Shirani, Ali Zayaan Macknojia, Wesley Miller and Diana Berman *

Department of Materials Science & Engineering, University of North Texas, Denton, TX 76203, USA; mohammadeskandari@my.unt.edu (M.E.)
* Correspondence: diana.berman@unt.edu; Tel.: +1-940-891-6778

Abstract: Protective coatings are important for enhancing tribological behavior, preventing surface degradation, and reducing friction-induced energy losses during the operation of mechanical systems. Recently, tribocatalytically driven formation of protective carbon films at the contact interface has been demonstrated as a viable approach for repairing and extending the lifetime of protective coatings. Here, we study the effect of catalytic metals, specifically their composition and amount, on the tribocatalysis process. To achieve this, we test the tribological performance of electro-deposited amorphous CoNiP and CoCuP coatings in different hydrocarbon-rich environments. Our results indicate that the tribocatalytic repair of wear-induced damage is optimal when Ni and Cu are included in the Co-P matrix at 5 wt% Ni and 7 wt% Cu, respectively. Characterization of the wear tracks suggests that among the considered samples, the tribofilms formed on the surface of Co7CuP have the highest concentration of graphitic carbon, leading to a more significant reduction in the COF and wear rate. The carbon tribofilm formation was more pronounced in decane and synthetic oil than in ethanol, which is attributed to the difference in the length of the hydrocarbon molecules affecting viscosity and the lubricant film thickness during boundary lubrication sliding.

Keywords: tribochemistry; carbon; zero wear; nickel; copper; catalysis; repair

Citation: Al Sulaimi, R.; Eskandari, M.; Shirani, A.; Macknojia, A.Z.; Miller, W.; Berman, D. Effect of Cu and Ni Inclusion on Tribological Performance of Tribocatalytically Active Coatings in Hydrocarbon Environments. *Coatings* **2024**, *14*, 61. https://doi.org/10.3390/coatings14010061

Academic Editor: Francisco J. G. Silva

Received: 8 December 2023
Revised: 22 December 2023
Accepted: 24 December 2023
Published: 31 December 2023

1. Introduction

Surface and interface degradation, along with friction-induced energy loss, are major factors contributing to failure of machines' components and increase in global carbon emissions [1]. Implementing effective lubrication techniques based on advanced liquid [2,3] and solid [4,5] lubricants and coating materials [6–8] and reducing friction can yield significant benefits, including cost savings, reduced waste, and environmental advantages. However, liquid lubricants are not always compatible with the requirements of the mechanical systems and the use of protective coatings offers a temporary solution to friction- and wear-related issues, since their lifetime is limited [8,9].

Recently, tribocatalysis [10], the process of in situ formation of lubricating and wear-reversing carbon films at the sliding interface induced by local heating [11,12], shear forces, and the presence of hydrocarbon sources and catalytic metals, has demonstrated its effectiveness in suppressing damage and wear [13–15]. The compatibility of tribocatalysis with a wide range of hydrocarbon gases or liquids acting as a source of carbon [16,17] and catalytic metals lowering the energy for hydrocarbon transformation [18] make the process highly attractive for various applications. The formation of protective carbon films through tribocatalysis is attractive for lowering frictional losses, since carbon-based films, such as, for example, graphene [19,20] or diamond-like carbon [21,22], enable easy shearing in an incommensurate state configuration [23–25].

Keeping this in mind, a number of recent studies have successfully demonstrated tribocatalytic activity at various material systems. Wohlgemuth [26] demonstrated the catalytic activity of a thin Pd layer on conventional milling equipment, while Shirani et al. [13]

found that Pt-Au films on noble alloy surfaces formed carbon-based tribofilms, reducing wear rate compared to 440 C HT steel. Recent investigations have highlighted the superior tribocatalytic activity and reactivity of longer-chain hydrocarbons, such as hexadecane, compared to shorter-chain counterparts [27–29]. Furthermore, evaluations of coatings and molecular dynamics simulations have shown that longer-chain n-alkanes reduce friction and enhance surface protection by facilitating the formation of uniform tribofilms and mono-layers in the asperity contact interface [29,30]. In all previous efforts, though, limited comparison across various catalytic systems has been performed, mostly due to the lack of a coating approach adaptable for the incorporation of different catalytic elements.

Electrochemically deposited cobalt-phosphorus coatings are attractive across various fields, including magnetic storage devices, hydrogen generation systems, and protective films [31]. Since the deposition conditions and material precursors can be easily manipulated to control the crystallinity and incorporation of additional elements into the coatings, amorphous Co-P coatings with inclusion of Pt have been proposed as a base for magnetic recording [32] or with inclusion of Ni as a base for hydrogen generation [33].

This study highlights the efforts in designing coatings that enhance the tribological performance of mechanical systems through activation of tribocatalytic activity. Specifically, the impact of catalytic materials, Cu and Ni, on the tribocatalysis behavior of Co-P-based amorphous coatings is examined. Cu and Ni are selected based on the previous studies demonstrating their promising characteristics as catalysts [34–37] and tribocatalysts [10,14,16]. Additionally, this study seeks to examine the universality of tribocatalysis for the formation of carbon-based tribofilms across hydrocarbon-rich environments and synthetic oils to evaluate their efficacy in reducing friction and wear.

2. Materials and Methods

2.1. Synthesis of CoP-Based Tribocatalytic Coatings

Electrodeposition was used to design a coating consisting of a Co-P matrix with the inclusion of Ni and Cu at different concentrations. For this, hardened (~60 HRC) and polished (~50 nm roughness) AISI 52100 steel substrates were initially rinsed with acetone followed by isopropanol, and then they were anodically cleaned for 3 min at 5 V in a solution containing 35 g/L NaOH, 25 g/L $NaCO_3$, and 1 g/L SDS to remove any residual greases and organic surface contaminations. The surfaces of the samples were then treated for several seconds (~20 s) using a diluted solution of sulfuric acid (10 wt% of sulfuric acid in DI water) at room temperature to improve the adhesion of the coating during the deposition. During the electrodeposition, a cobalt electrode and an AISI 52100 substrate were used as the anode and the cathode, respectively. For surface activation, after being anodically cleaned using the same procedure described for the substrates, the anode was submerged in 1:1 solution of HCl in DI water and sonicated for 30 s at room temperature. The electrolyte bath used for the coating deposition was prepared by mixing $CoCl_2$ as the source of Co metal (210 g/L), H_3PO_4 as the phosphorus source (50 g/L), sodium hypophosphate as the reducing agent (20 g/L), and sodium saccharin as a leveler and a brightener (1 g/L). The pH of the bath was kept at 1.5 at 80 °C. Different quantities of nickel chloride and copper (II) chloride were added to the bath to facilitate formation of Co-Ni-P and Co-Cu-P coatings as shown in Table 1. The thickness of the resulting coatings was approximately 12 µm, controlled by the deposition time. This thickness was selected to provide protection to the surface while not impacting the mechanical characteristics of the substrate responsible for the contact formation.

Table 1. Summary of the resulting composition of the coatings.

	$NiCl_2$ (g/L)	$CuCl_2$ (g/L)	Ni (wt%)	Cu (wt%)	P (wt%)
CoP	0	0	0	0	12.5
Co5NiP	10	0	4.9	0	12.2
Co7NiP	20	0	7.4	0	11.3
Co5CuP	0	0.5	0	4.8	11.6
Co7CuP	0	1	0	6.8	11.2

2.2. Tribological Analysis

The tribological analysis tests were performed in an macroscale pin-on-disk tribometer (Anton Paar, Graz, Austria) in a reciprocating mode. The temperature during the tests was kept at 50 °C, selected based on the earlier studies showing increased tribocatalytic activity in an ethanol environment under such conditions [13]. All the tests were performed using AISI 52100 steel flats (McMaster Carr, Elmhurst, IL, USA), 1 inch (25.4 mm) in diameter, uncoated or coated; and AISI 52100 steel balls, 6 mm in diameter, purchased from McMaster Carr. The experiments were conducted at 2 Hz, with a stroke length of 1.4 mm, leading to a maximum linear speed of 0.88 cm/s. The tests were performed under applied normal loads, and the corresponding maximum Hertzian contact pressures were 0.5 N (0.33 GPa), 1 N (0.42 GPa), 2 N (0.53 GPa), and 5 N (0.71 GPa). The maximum Hertzian contact pressure was calculated using Equation (1):

$$P_o = \frac{1}{\pi}\left(\frac{6FE^{*2}}{R^2}\right)^{\frac{1}{3}} \quad (1)$$

where P_o is the maximum contact pressure, F is the applied load, and R is the radius of the counter body. Also, E^* equals:

$$\frac{1}{E^*} = \frac{1-v_1^2}{E_1} + \frac{1-v_2^2}{E_2} \quad (2)$$

with E_1 and E_2 being the elastic moduli, and v_1 and v_2 being the Poisson's ratio for two surfaces in contact.

Three different liquid lubricants were used as a source of hydrocarbons, namely, decane, ethanol, and polyalphaolefin (PAO4). The lubricants were selected to assess the tribocatalytic mechanism across different environments and unravel their effect on the nature of the tribofilm. Variations in the molecular structure and thus the characteristics of the lubricants were expected to impact tribofilm formation by affecting the contact pressure needed for the dissociation of the hydrocarbon molecules. During the tests, the samples were covered with 60 cc of lubricant.

2.3. Characterization

Analysis of the chemical modifications induced by sliding was performed using an FEI Nova 200 NanoLab scanning electron microscope (SEM) equipped with an energy-dispersive X-ray spectroscope (EDS) (KNI Lab at Caltech, Pasadena, CA, USA). A Zeiss optical microscope was used to visualize the wear tracks and counter body wear. The structure of the coatings, specifically the phases, were analyzed with Rigaku Ultima III X-ray powder diffractometry (XRD) (Rigaku Americas Corporation, The Woodlands, TX, USA) using Cu Kα radiation scanned from 20–90° with a step size of 0.02° and a scan rate of 1°/min.

Raman spectroscopy analysis was performed using a Renishaw Raman spectrometer (Renishaw, Wotton-under-Edge, UK) equipped with a green laser at a wavelength of 532 nm. For the 2D mapping, acquisition of the individual spectra was performed with a ±10 nm accuracy for the position of a stage. The power of the laser and the exposure time were adjusted to minimize the heating, and thus any possible material transformations, of the samples during the analysis.

A Filmetrics optical interferometer (KLA Instruments, Milpitas, CA, USA) was used for the 3D profiling of the wear of the samples after the tests.

An INano nanoindenter (KLA Instruments, Milpitas, CA, USA) was used for analyzing changes to the hardness and elastic modulus of the coatings. For this, the hardness values were collected independently for each indent and then formatted in the form of 2D maps to represent changes in the mechanical behavior inside and outside the wear tracks.

X-ray photoelectron spectroscopy (XPS) data acquisition was performed with a PHI 5000 Versaprobe spectrometer (ULVAC-PHI, Kanagawa, Japan) with monochromatic 1486.6 eV Al

Kα radiation with an energy resolution of 0.1 eV. The samples were mounted using copper tape to improve the electrical conductivity at the surfaces. All the binding energies were rechecked using the C 1s peak at 284.5 eV.

3. Results

3.1. Characterization of the Deposited Coatings

Two sets of coatings were deposited electrochemically when tuning the content of the metallic elements in the electrolyte. The first set used adjustments to the Co^{+2}/Ni^{+2} ratio to synthesize Co5NiP (~5 wt% of Ni) and Co7NiP (~7 wt% of Ni) coatings. Such concentrations were selected based on our prior work demonstrating improvement in mechanical and tribological characteristics [38]. For the direct comparison of the effect of the nature of the catalytic elements, the second set employed adjustment in the Co^{+2}/Cu^{+2} ratio to synthesize Co5CuP (~5 wt% of Cu) and Co7CuP (~7 wt% of Cu) coatings. An electro-deposited amorphous Co-P coating without inclusion of Cu or Ni was used as a reference sample. To sustain the amorphous nature of the coating, the P-content was regulated by adjusting the current density during the electro-deposition process within the range of 11–12 wt%. Table 1 summarizes the amount of $NiCl_2$ and $CuCl_2$ used to generate each composition and the composition of the resulting coatings. Copper exhibits a higher deposition rate compared to nickel due to its lower overpotential [39]. This characteristic of copper explains the utilization of a lower concentration of $CuCl_2$ in the electro-deposition process for Co-Cu-P coatings.

Figure 1a reveals the XRD patterns for the electro-deposited coatings. A wide peak observed at 45° confirms the mostly amorphous nature of Co-P coatings, since the rapid cooling rate during the electro-deposition restricts rearrangement of atoms and higher phosphorus content prevents the Co atoms from attaining the thermodynamically stable crystalline structure [40]. Figure 1b,c show the cross-sectional SEM images and corresponding elemental maps for (b) Co5NiP and (c) Co5CuP coatings confirming their uniformity and structural integrity. The film thickness was measured at 12 µm +/− 0.5.

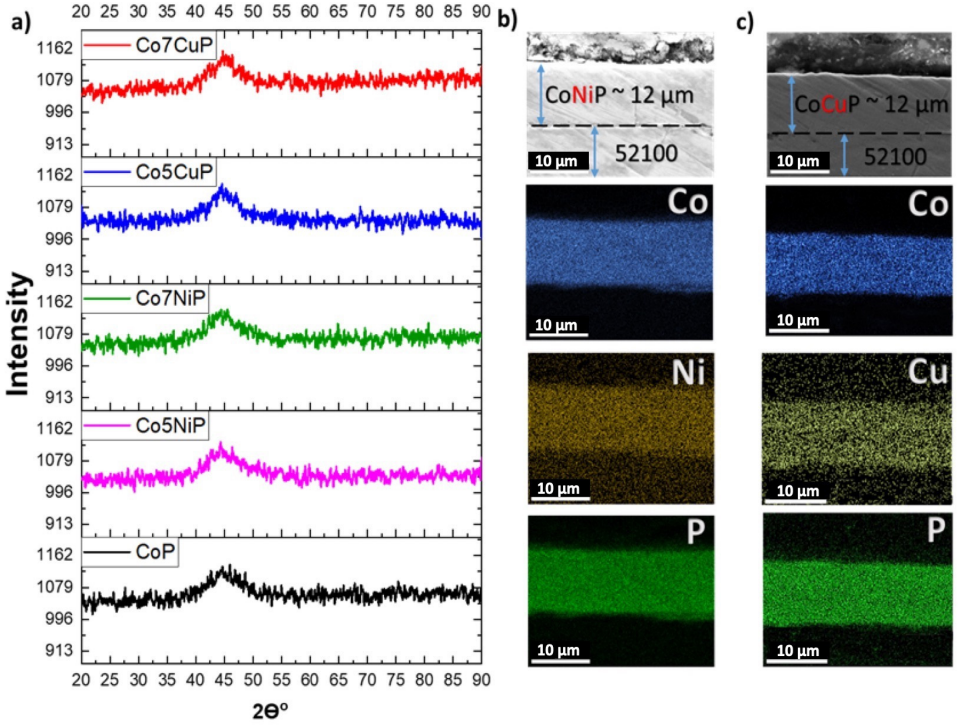

Figure 1. (**a**) XRD data for the deposited coatings. Cross-sectional SEM/EDS images for (**b**) Co5NiP and (**c**) Co5CuP films.

3.2. Effect of the Composition and Environment on Tribological Behavior

The coatings underwent testing in two distinct low-viscosity fuels, as they represent prospective fuel alternatives for advanced, high-efficiency combustion engines. Additionally, the coatings were subjected to testing with PAO4, given its significance in conventional mechanical systems as a base oil lubricant. Table 2 summarizes the dynamic viscosity values for all three lubricants at 50 °C, used during the following tribological tests.

Table 2. Dynamic viscosity values for lubricants at 50 °C [41–44].

Lubricant	Ethanol	Decane	PAO4
Viscosity at 50 °C (mPA·s)	1.14	0.85	32.0

The findings derived from the tribological experiments offered valuable insights into the frictional characteristics of the coatings incorporating Ni and Cu (Figure S1). The evaluation was performed in comparison to uncoated AISI 52100 steel substrate and the steel substrate with amorphous Co-P coating. The coefficient of friction (COF) and the wear rate values are summarized in Figure 2. The results are presented for the loads demonstrating the most evident contrast for each of the lubricants (0.5 N for ethanol, 2 N for decane, and 5 N for PAO4).

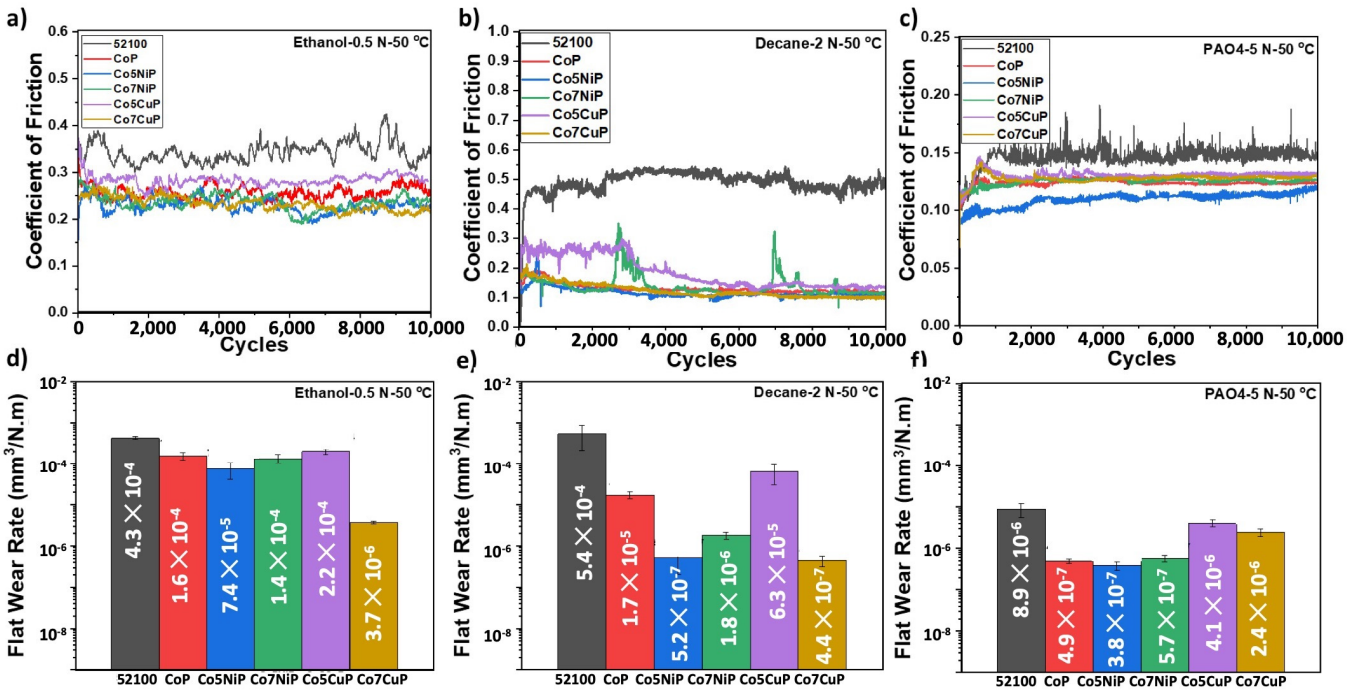

Figure 2. Coefficient of friction of the coatings and an uncoated AISI 52100 steel in (**a**) ethanol, 0.5 N, (**b**) decane, 2 N, (**c**) PAO4, 5 N. The flat wear rate values of (**d**) ethanol, 0.5 N, (**e**) decane, 2 N, (**f**) PAO4, 5 N at 50 °C.

The COF value for uncoated steel samples tested in ethanol was around 0.40 (Figure 2a), leading to a wear rate of ~4.3 × 10^{-4} mm^3/N m (Figure 2d). Nevertheless, the inclusion of Ni in the amorphous Co-P composition led to Co-5Ni-P displaying lower values for both coefficient of friction (COF) and wear rate compared to Co-7Ni-P. On average, Co-5Ni-P exhibited a COF value of 0.23. Additionally, the introduction of 7 wt% Cu to the Co-P film significantly enhanced the coating's protection and elevated wear resistance. This not only led to decreased friction but also resulted in a wear rate reduction by two orders of magnitude compared to the coating with 5 wt% Cu.

When the tribological experiments were conducted in decane, the average coefficient of friction (COF) for all coatings decreased to 0.14, as depicted in Figure 2b, contributing to the reduction in wear, as illustrated in Figure 2e. This decline can be ascribed to the differing chemical and physical attributes of decane when compared to ethanol. The extended hydrocarbon chain in decane facilitates the establishment of more robust intermolecular forces [44]. This leads to the formation of a lubricating film that is thicker and more resilient. Such a quality enhances the lubricating effectiveness of decane when juxtaposed with ethanol, which possesses a shorter chain and provides weaker protection to the underlying surfaces, potentially resulting in less efficient lubrication. Additionally, decane has demonstrated superiority as a low-viscosity fuel, as indicated by its enhanced engine performance [45].

As depicted in Figure 2b,e, the behavior of the coating follows a comparable pattern to what was observed in ethanol. Of the copper-containing coatings, Co7CuP outperforms Co5CuP, showcasing superior wear resistance, as indicated by its markedly lower flat wear rate of 4.37×10^{-7} mm^3/N m, three orders of magnitude lower than the wear rate for uncoated steel samples. Research has demonstrated that the addition of Cu to alloys results in several beneficial effects. Cu improves hardness and impact toughness [46] and enhances wear resistance [47]. For example, in steels, the addition of copper encourages martensite formation, thus increasing hardness, or helps to retain austenite phase, thus impacting toughness [46,47]. In other alloys, Cu reinforces the materials through solid solution formation [48].

The tribological characteristics of the coatings in PAO4, a commonly used low-viscosity base oil in industrial applications, are summarized in Figure 2c,f. The results suggest that the oil forms a lubricating film for all the tested tribopairs, leading to relatively low friction regime. The higher viscosity of PAO4 compared to the low-viscosity fuels examined in this study ensures smooth flow and strong adhesion to the coating surface during applied loads. The COF value for the uncoated AISI 52100 steel is notably higher than the COFs for the coatings (~by 10–12%). Interestingly, in contrast to ethanol and decane, the addition of Ni results in better wear resistance than the addition of Cu. Even more, the addition of Cu to the CoP matrix resulted in a worsening of the coatings' performance, suggesting that in the case of PAO4, the Cu-activated tribochemical activity is not efficient in providing surface protection. It should be noted that observed wear rates are at least one order of magnitude lower than those reported in the literature for CoP coatings [49].

The results obtained with optical profilometry (Figure 3) affirm the findings presented in Figure 2. Regarding the wear track depth, the uncoated steel displays a significant wear profile with a depth of approximately 4 μm when tested in decane (Figure 3b). In contrast, CoMeP coatings yield comparatively shallow wear tracks, with a depth measuring below 1 μm in (Figure 3a,b), where Me is the catalytic metal added to the amorphous CoP matrix.

In addition to manifesting a decreased wear rate, Co5NiP displays the lowest depth in the profilometry data. This observation implies that the 5 wt% Ni coating attains an optimal tribofilm formation regime during sliding in alkane-based and alcohol-based environments serving as sources of hydrocarbons. A thorough examination of the experimental data reveals that the introduction of 7 wt% Ni has detrimental effects on the coating's tribological performance. This can be ascribed to the impact of increased Ni content on the mechanical characteristics of the coating. With a higher Ni concentration, the coating's hardness rises, subsequently reducing its ductility. As a result, the coating becomes more prone to cracking and deformation under sliding contact.

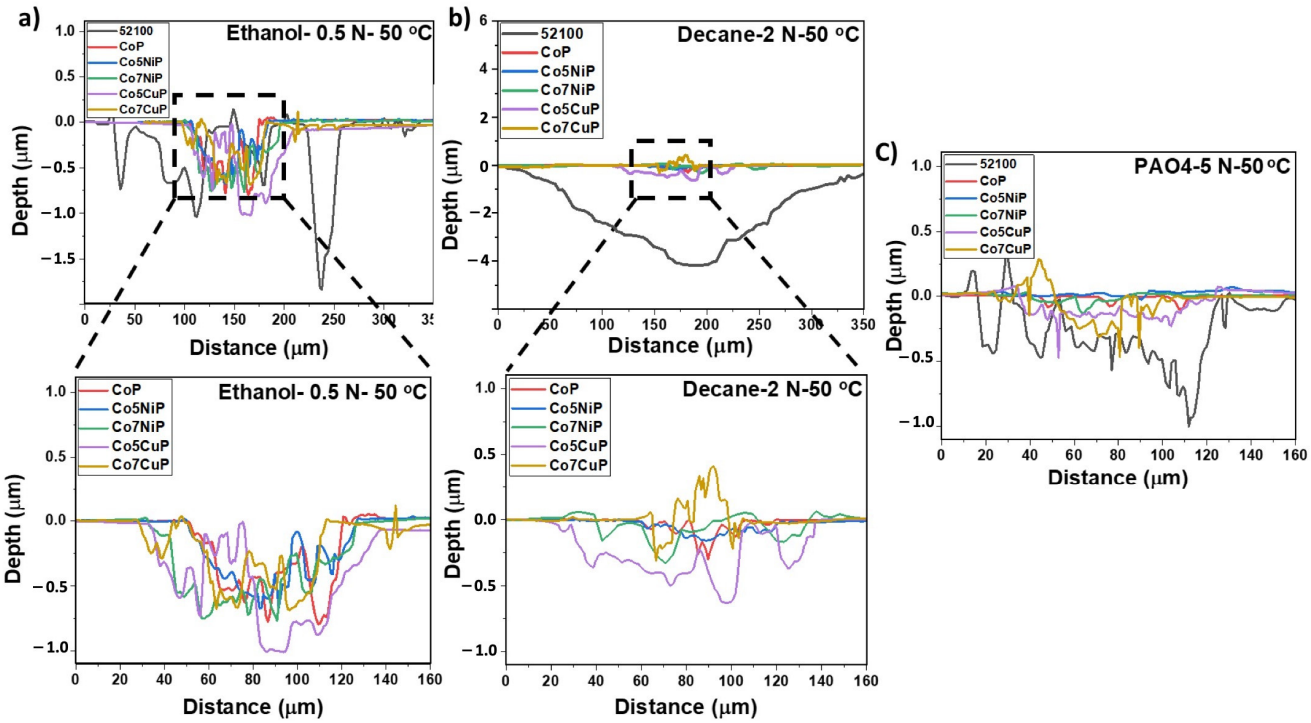

Figure 3. Optical profilometry results for the wear track depth profiles captured at the center of the wear tracks after the tests performed in (**a**) ethanol at 0.5 N, (**b**) decane at 2 N, and (**c**) PAO4 at 5 N.

3.3. Comparative Analysis of Co5NiP and Co7CuP

In the preceding findings, Co5NiP and Co7CuP emerged as the top-performing coatings in terms of wear resistance and the creation of carbon-based tribofilm. Consequently, these two coatings were selected for a detailed comparative analysis. Figure 4 provides an overview of their tribological behavior in low-viscosity fuels and PAO4 base oil.

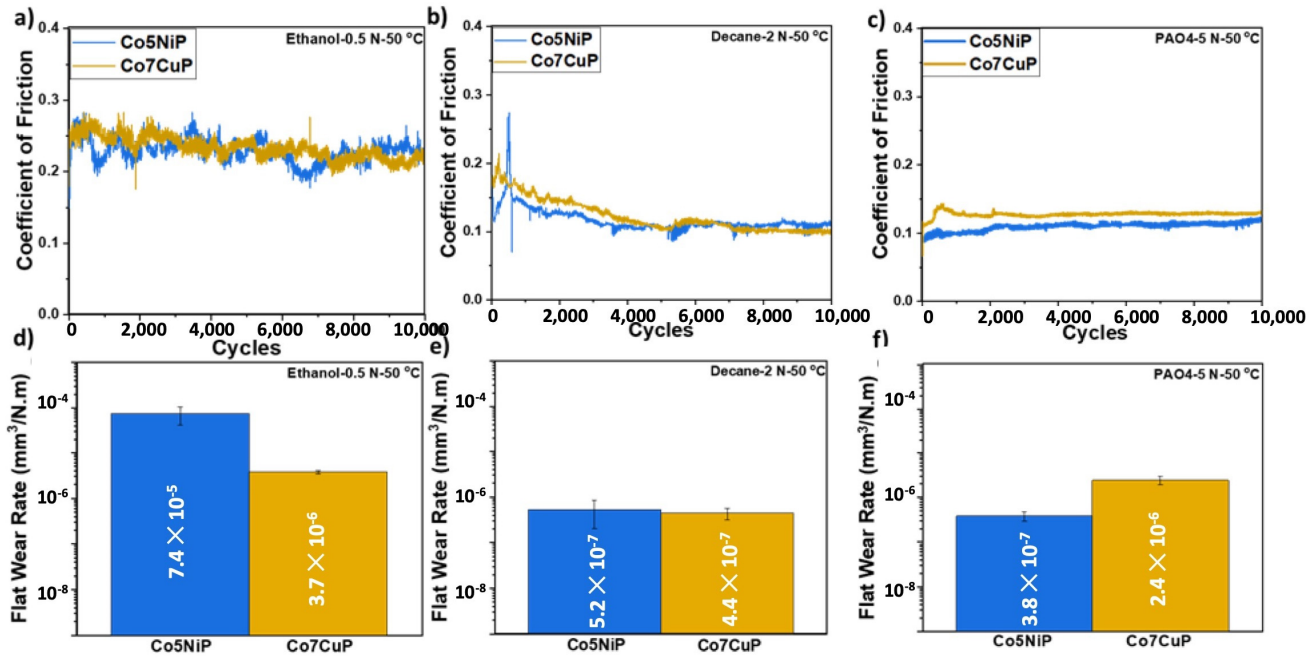

Figure 4. Coefficient of friction of Co5NiP and Co7CuP in (**a**) ethanol at 0.5 N, (**b**) decane at 2 N, and (**c**) PAO4 at 5 N. The flat wear rate values in (**d**) ethanol at 0.5 N, (**e**) decane at 2 N, and (**f**) PAO4 at 5 N at 50 °C.

The incorporation of ethanol, in the vicinity of the catalysts Cu and Ni, initiated the formation of carbon-based films that successfully mitigated friction and wear within the sliding interfaces. Remarkably, Co7CuP demonstrated enhanced wear resistance in low-viscosity fuels, a characteristic attributed to the elevated surface energy and catalytic activity of Cu when interacting with organic molecules [50,51].

The surface energy promotes better adhesion of carbon-based films, further enhancing the reduction of friction and wear in the system, and the catalytic activity accelerates dehydrogenation and scission of the bonds in hydrocarbon molecules. In the case of PAO4, (Figure 4c,f), the results indicate that the effect of oil lubricity was enhanced by tribofilm formation for Co5NiP coating.

Figure 5 shows variation in the hardness value across the wear tracks with the corresponding optical profilometry images. For PAO4, the Co5NiP coating demonstrated fewer fluctuations in the hardness values across the wear track in contrast to the Co7CuP. The variations in hardness values within the wear tracks are attributed to two distinct phenomena occurring during the sliding process. Regions exhibiting lower hardness values (<6 GPa) indicate the development of a carbon-based tribofilm. Conversely, higher hardness values (>6 GPa) are linked to grain refinement and, to some degree, to the formation of oxide layers, as substantiated by the elemental mapping images presented in Figure 6. Despite contributing to increased hardness, this native oxide layer is less effective in reducing wear and minimizing friction. Interestingly, for the PAO4 tests, the maps do not show such large fluctuations in hardness as for ethanol and decane. This observation suggests that the higher viscosity of the oil is responsible for the formation of a protective boundary layer that acts as a barrier limiting the oxygen molecules from forming oxide layers. The tribocatalytic activity seems to be less pronounced as well. Analysis of the changes in elastic modulus inside the wear track (Figure S2) suggested similar response by the materials to the load and shear, though the observed variations in the elastic modulus are not as pronounced. Interestingly, the variation is minimal for Ni-containing coatings.

The analysis conducted through Raman spectroscopy, in conjunction with 2D elemental mapping (EDS) as depicted in Figure 6, indicates that the source of the favorable tribological properties of the coating lies in the in situ development of a carbon-rich tribofilm. In all tested systems (ethanol, decane, and PAO4), the presence of firmly adhered carbon patches was observed, with their concentrations progressively increasing toward the peripheries of the wear track.

Raman spectroscopy findings suggest that these carbon layers exhibit a combination of D (at approximately 1351 cm^{-1}) and G (at approximately 1580 cm^{-1}) bands, characteristic of amorphous carbon structures, consistent with our earlier research [13]. The minor fluctuation in the relative intensity of D and G peaks is ascribed to a greater prevalence of incompletely converted tribopolymers, stemming from the fragments of ethanol molecules, as opposed to decane molecules [52].

In the case of Co7CuP (Figure 7), the carbon-based nature of the formed tribofilms is also summarized with EDS and Raman maps. Interestingly, the Raman results indicate that the nature of the carbon peaks varies depending on the coating composition and the hydrocarbon source [52].

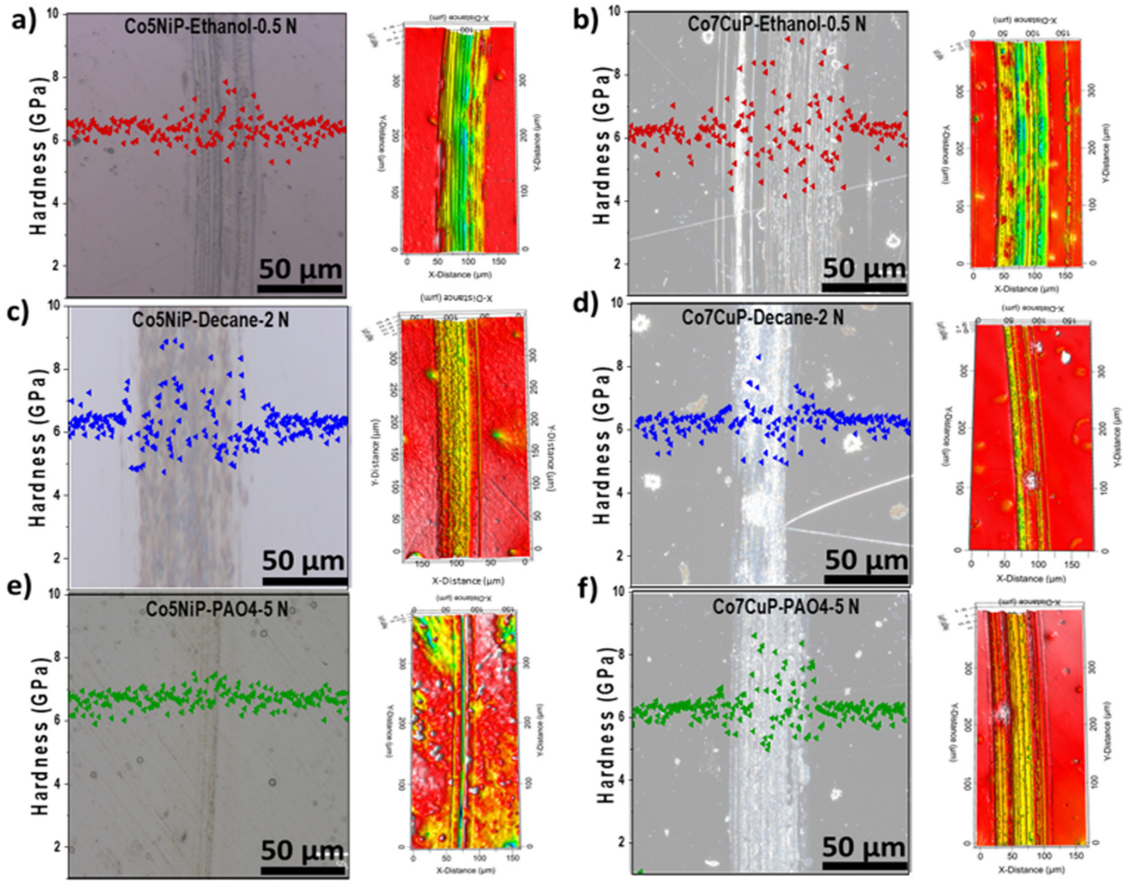

Figure 5. Nanoindentation hardness mapping on the wear tracks for Co5NiP in (**a**) ethanol, 0.5 N, (**c**) decane, 2 N, (**e**) PAO4, 5 N tests; and Co7CuP for (**b**) ethanol, 0.5 N, (**d**) decane, 2 N, (**f**) PAO4, 5 N tests. 3D images generated by the optical profilometer.

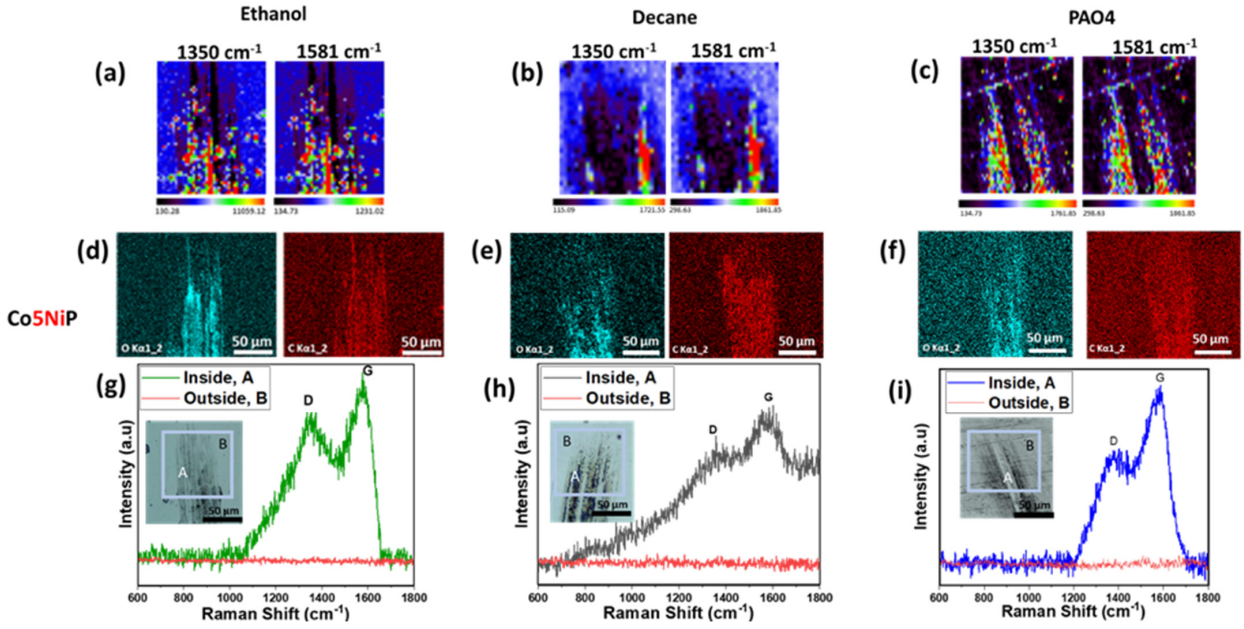

Figure 6. (**a**–**c**) Raman maps of Co5NiP wear track in ethanol, decane, and PAO4; (**d**–**f**) EDS maps of Co5NiP wear track in ethanol, decane, and PAO4; (**g**–**i**) Raman spectra (with characteristics D and G carbon peaks) inside the wear track of Co5NiP in ethanol, decane, and PAO4. The points A and B used for collecting spectra inside and outside the weartracks are highlighted in the SEM images included as insets.

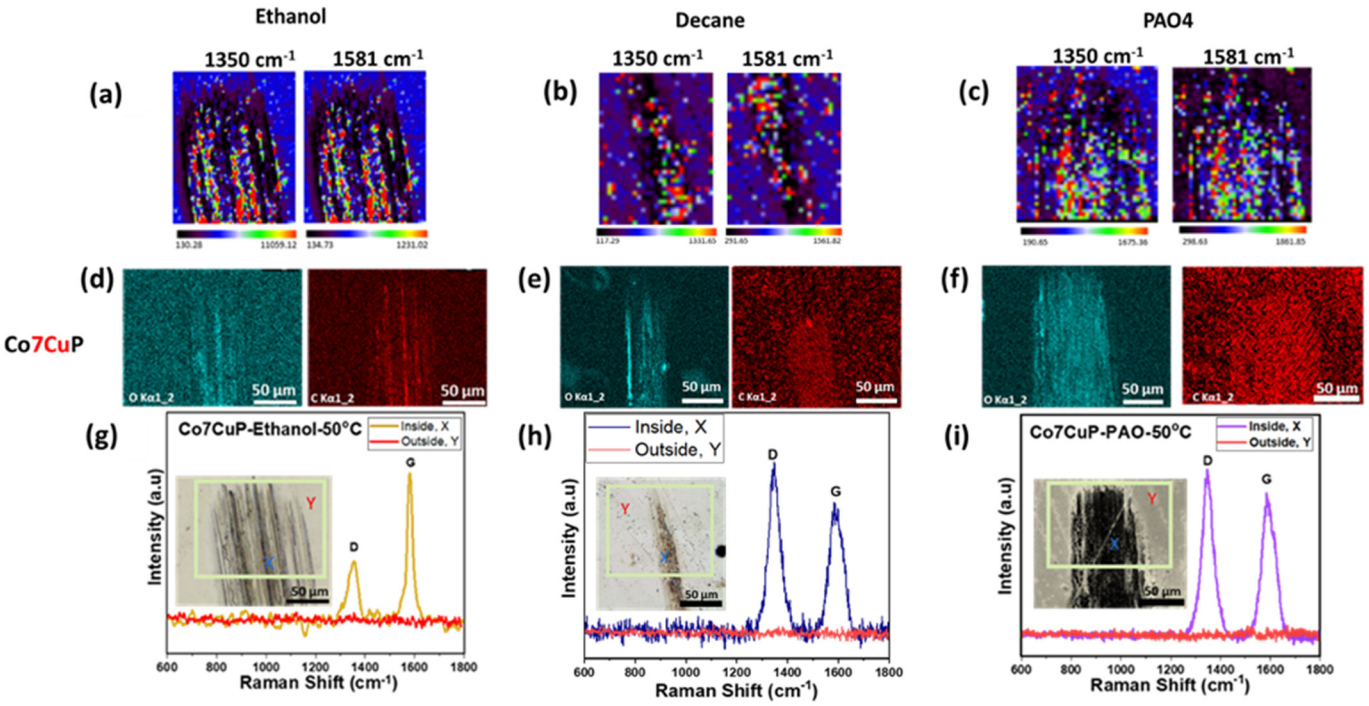

Figure 7. (**a**–**c**) Raman maps of Co7CuP wear track in ethanol, decane, and PAO4; (**d**–**f**) EDS maps of Co7CuP wear track in ethanol, decane, and PAO4; (**g**–**i**) Raman spectra (with characteristics D and G carbon peaks) inside the wear track of Co7CuP in ethanol, decane, and PAO4. The points X and Y used for collecting spectra inside and outside the weartracks are highlighted in the SEM images included as insets.

To further evaluate the variability in the carbon formation, we summarized the changes in the characteristic carbon peaks. Table 3 presents a comparison of full-width half-maximum (FWHM) values for characteristic D (aat ~1350 cm^{-1}) and G (at ~1560 cm^{-1}) peaks. Interestingly, the results suggest that Co7CuP is likely to form more sp^2-bonded carbon layers, supposedly of a graphitic nature, than Co5NiP. In the case of Co5NiP, high full-width half-maximum (FWHM) values for D and G peaks suggest more amorphous, DLC-like structure of the carbon layers. Prior studies indicated that comparison of Raman D and G relative ratios as well as FWHM of the D and G peaks can be used to resolve the sp^2 vs. sp^3 nature of carbon bonding [53]. Another interesting observation is that an increase in the hydrocarbon chain length leads to widening of the D and G peaks for Cu-based samples, which suggests that the number of defects increases as a result of not complete scission of the hydrocarbon chains. Meanwhile, in the case of Ni-based films, there is no clear correlation between the hydrocarbon chain length and the changes in the FWHM of D and G peaks.

Table 3. FWHM of the D and G peaks from Raman spectra of Co5NiP and Co7CuP in decane, ethanol, and PAO4.

Lubricant	Coating	D-Band FWHM, cm^{-1}	G-Band FWHM, cm^{-1}
Ethanol	Co5NiP	100 ± 8	104 ± 12
Ethanol	Co7CuP	47 ± 6	26 ± 7
Decane	Co5NiP	101 ± 6	103 ± 12
Decane	Co7CuP	53 ± 7	68 ± 8
PAO4	Co5NiP	98 ± 12	102 ± 9
PAO4	Co7CuP	70 ± 14	78 ± 12

To further understand the difference between the formed tribofilms, we performed XPS analyses of the wear tracks. Figure 8 summarizes the observed C1s, O1s, and Ni2p and Cu2p (depending on the sample) peaks. In the case of the tribofilms formed on Ni-based coatings, C1 spectra, in addition to C-C bonding at 284.5 eV, show the second peak shifting from 287.5 eV for ethanol to 286 eV for PAO4. At the same time, the intensity of the Ni2p peak increases, suggesting a higher presence of Ni in the tribofilms formed from PAO4 than those formed from ethanol. This observation suggests that PAO4 conversion requires more Ni to be pulled from the coating to assist in the tribocatalytic reaction. In the case of Cu-based films, the C1 spectra show no distinguished satellite peaks, only the major peak at 284.5 eV, further supporting the previous conclusion that Cu facilitates formation of more sp^2-bonded carbon.

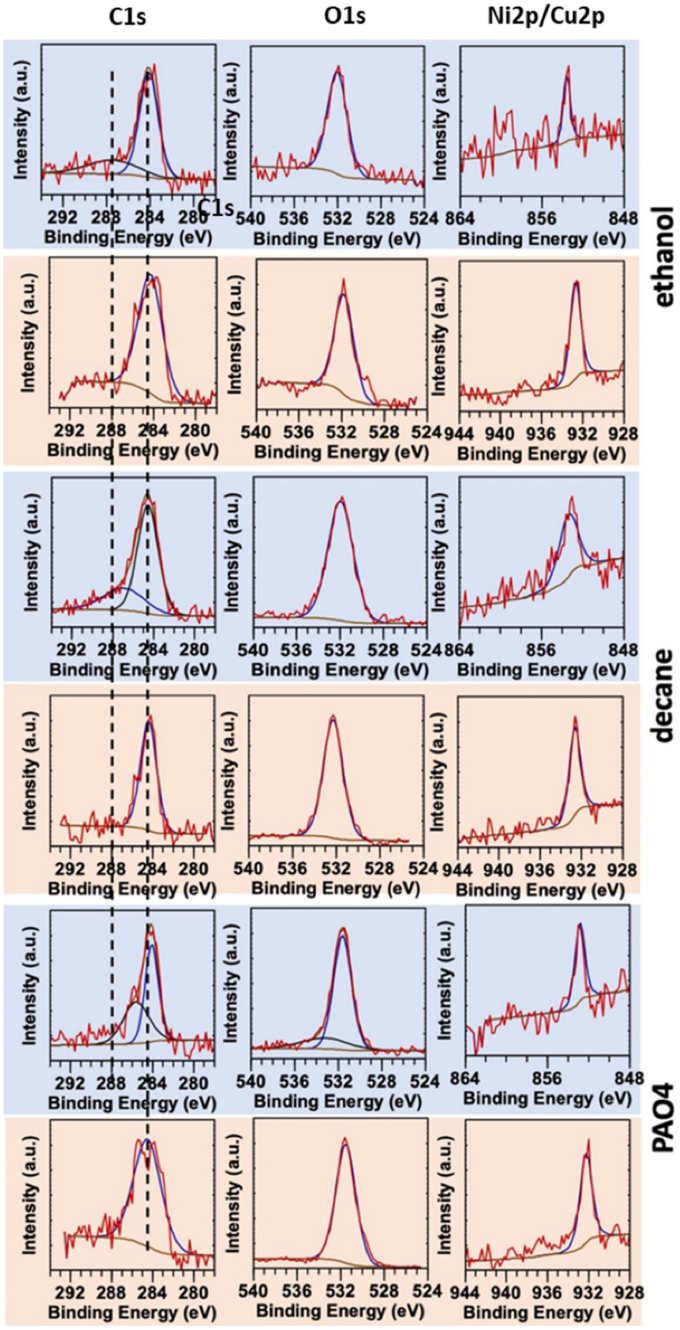

Figure 8. XPS analysis of the wear tracks formed on Ni-based (highlighted in blue) and Cu-based (highlighted in orange) samples in different environments.

As widely seen in the literature, both types of carbon films provide good protection of the surfaces [20,22]. However, the sp^2-bonded carbon films seem to provide easier shearing and better protection in low-viscosity hydrocarbons. Meanwhile, the more amorphous nature of carbon films is beneficial for sliding in PAO4 and results in lower COF and better protection of the Co5NiP surface from damage.

4. Conclusions

The study focused on the development and enhancement of coatings to improve the tribological performance of mechanical systems operated in various hydrocarbon-rich environments. The study investigated the effects of composition and content of catalytic materials on the tribocatalysis behavior of CoP-based coatings. Two sets of coatings with different inclusions of Ni and Cu were electro-deposited by adjusting the quantities of metallic precursors in the electrolyte. The coatings exhibited amorphous nature ensured with ~12 wt% of P and a uniform distribution of constituent elements across 12 μm thickness.

Tribological experiments were conducted using low-viscosity fuels, ethanol and decane, and a synthetic oil, PAO4, to evaluate the effect of the hydrocarbon source on the protective tribofilm formation. The COF and wear rate values were measured and compared to those of uncoated AISI 52100 steel and an amorphous CoP coating. The results demonstrated that the inclusion of catalytic elements, such as Ni and Cu, improved the protection and wear resistance of the coating. Co5NiP exhibited lower COF and wear rate values compared to Co7NiP, while Co7CuP outperformed Co5CuP, showing significantly lower friction and wear rates.

Characterization using optical profilometry, nanoindentation hardness mapping, EDS, Raman spectroscopy, and XPS confirmed the formation of carbon-based tribofilms on the surfaces of the coating during sliding. Co7CuP demonstrated the best performance in decane and ethanol, which was attributed to the formation of more graphitic carbon film, while Co5NiP improved the friction and wear in presence of PAO4, promoting growth of the amorphous carbon film.

Overall, the research findings highlight the importance of composition and catalyst elements in enhancing the tribological performance of coatings and promoting the formation of carbon-based tribofilms. The study provides valuable insights into the behavior of coatings in different lubricating environments and contributes to the development of improved lubrication strategies for mechanical systems.

Supplementary Materials: The following supporting information can be downloaded at: https://www.mdpi.com/article/10.3390/coatings14010061/s1, Figure S1: Summary of the coefficient of friction analysis used for optimization of the test parameters for different coatings in ethanol, decane, and PAO4. Figure S2: Nanoindentation modulus mapping on the wear tracks for Co5NiP in (a) ethanol, 0.5 N, (c) decane, 2 N, (e) PAO4, 5 N tests, and Co7CuP for (b) ethanol, 0.5 N, (d) decane, 2 N, (f) PAO4, 5 N tests.

Author Contributions: Conceptualization, D.B.; methodology, D.B. and A.S.; validation, R.A.S., M.E. and A.Z.M.; formal analysis, R.A.S., M.E., A.Z.M. and W.M.; investigation, R.A.S., M.E. and A.Z.M.; resources, D.B.; data curation, R.A.S., M.E., A.Z.M., W.M. and D.B.; writing—original draft preparation, R.A.S., M.E. and D.B.; writing—review and editing, D.B.; supervision, D.B.; funding acquisition, D.B. All authors have read and agreed to the published version of the manuscript.

Funding: The authors acknowledge the support of this work by the National Science Foundation (NSF) (Awards No. 2018132 and No. 2323452).

Institutional Review Board Statement: Not applicable.

Informed Consent Statement: Not applicable.

Data Availability Statement: The authors confirm that the data supporting the findings of this study are available within the article.

Acknowledgments: This work was performed in part at the University of North Texas' Materials Research Facility.

Conflicts of Interest: The authors declare no conflict of interest.

References

1. Holmberg, K.; Andersson, P.; Erdemir, A. Global energy consumption due to friction in passenger cars. *Tribol. Int.* **2012**, *47*, 221–234. [CrossRef]
2. Al Sulaimi, R.; Macknojia, A.; Eskandari, M.; Shirani, A.; Gautam, B.; Park, W.; Whitehead, P.; Alonso, A.P.; Sedbrook, J.C.; Chapman, K.D.; et al. Evaluating the effects of very long chain and hydroxy fatty acid content on tribological performance and thermal oxidation behavior of plant-based lubricants. *Tribol. Int.* **2023**, *185*, 108576. [CrossRef]
3. Somers, A.E.; Howlett, P.C.; Macfarlane, D.R.; Forsyth, M. A review of ionic liquid lubricants. *Lubricants* **2013**, *1*, 3–21. [CrossRef]
4. Sunil, T.; Sandeep, M.; Kumaraswami, R.; Shravan, A. A critical review on solid lubricants. *Int. J. Mech. Eng. Technol.* **2016**, *7*, 193–199.
5. Macknojia, A.; Ayyagari, A.; Zambrano, D.; Rosenkranz, A.; Shevchenko, E.V.; Berman, D. Macroscale Superlubricity Induced by MXene/MoS_2 Nanocomposites on Rough Steel Surfaces under High Contact Stresses. *ACS Nano* **2023**, *17*, 2421–2430. [CrossRef] [PubMed]
6. Breton, O.K.; Handzel, E.J.; Tennant, J.M. Process for Making Wear-Resistant Coatings. U.S. Patent 6,649,682, 18 November 2003.
7. Mroczkowski, S.J. Multi-Layer Wear Resistant Coatings. *Ausz. Aus Den Eur. Patentanmeldungen Teil I* **1990**, *6*, 2595.
8. Chu, J.P.; Jang, J.; Huang, J.; Chou, H.; Yang, Y.; Ye, J.; Wang, Y.; Lee, J.; Liu, F.; Liaw, P.; et al. Thin film metallic glasses: Unique properties and potential applications. *Thin Solid Films* **2012**, *520*, 5097–5122. [CrossRef]
9. Awang, M.; Khalili, A.A.; Pedapati, S.R. A review: Thin protective coating for wear protection in high-temperature application. *Metals* **2019**, *10*, 42. [CrossRef]
10. Berman, D.; Erdemir, A. Achieving Ultralow Friction and Wear by Tribocatalysis: Enabled by *In-Operando* Formation of Nanocarbon Films. *ACS Nano* **2021**, *15*, 18865–18879. [CrossRef]
11. Ashby, M.F.; Abulawi, J.; Kong, H.S. Temperature Maps for Frictional Heating in Dry Sliding. *Tribol. Trans.* **1991**, *34*, 577–587. [CrossRef]
12. Junbin, Y.; Junxiu, D. Tribocatalysis reaction during antiwear synergism between borates and Sn(IV) compounds in boundary lubrication. *Tribol. Int.* **1996**, *29*, 429–432. [CrossRef]
13. Shirani, A.; Li, Y.; Smith, J.; Curry, J.; Lu, P.; Wilson, M.; Chandross, M.; Argibay, N.; Berman, D. Mechanochemically driven formation of protective carbon films from ethanol environment. *Mater. Today Chem.* **2022**, *26*, 101112. [CrossRef]
14. Erdemir, A.; Ramirez, G.; Eryilmaz, O.L.; Narayanan, B.; Liao, Y.; Kamath, G.; Sankaranarayanan, S.K.R.S. Carbon-based tribofilms from lubricating oils. *Nature* **2016**, *536*, 67–71. [CrossRef] [PubMed]
15. Jacques, K.; Shirani, A.; Smith, J.; Scharf, T.W.; Walck, S.D.; Berkebile, S.; Eryilmaz, O.L.; Voevodin, A.A.; Aouadi, S.; Berman, D. MoVN-Cu Coatings for In Situ Tribocatalytic Formation of Carbon-Rich Tribofilms in Low-Viscosity Fuels. *ACS Appl. Mater. Interfaces* **2023**, *15*, 30070–30082. [CrossRef] [PubMed]
16. Ramirez, G.; Eryilmaz, O.L.; Fatti, G.; Righi, M.C.; Wen, J.; Erdemir, A. Tribochemical Conversion of Methane to Graphene and Other Carbon Nanostructures: Implications for Friction and Wear. *ACS Appl. Nano Mater.* **2020**, *3*, 8060–8067. [CrossRef]
17. Hsu, S.M.; Zhang, J.; Yin, Z. The Nature and Origin of Tribochemistry. *Tribol. Lett.* **2002**, *13*, 131–139. [CrossRef]
18. Argibay, N.; Babuska, T.; Curry, J.; Dugger, M.; Lu, P.; Adams, D.; Nation, B.; Doyle, B.; Pham, M.; Pimentel, A.; et al. In-situ tribochemical formation of self-lubricating diamond-like carbon films. *Carbon* **2018**, *138*, 61–68. [CrossRef]
19. Soldano, C.; Mahmood, A.; Dujardin, E. Production, Properties and Potential of Graphene. *Carbon* **2010**, *48*, 2127–2150. [CrossRef]
20. Chen, X.; Li, J. Superlubricity of carbon nanostructures. *Carbon* **2020**, *158*, 1–23. [CrossRef]
21. Ayyagari, A.; Alam, K.I.; Berman, D.; Erdemir, A. Progress in Superlubricity Across Different Media and Material Systems—A Review. *Front. Mech. Eng.* **2022**, *8*, 908497. [CrossRef]
22. Tyagi, A.; Walia, R.; Murtaza, Q.; Pandey, S.M.; Tyagi, P.K.; Bajaj, B. A critical review of diamond like carbon coating for wear resistance applications. *Int. J. Refract. Met. Hard Mater.* **2019**, *78*, 107–122. [CrossRef]
23. Liu, Y.; Ge, X.; Li, J. Graphene lubrication. *Appl. Mater. Today* **2020**, *20*, 100662. [CrossRef]
24. Gao, Q.; Liu, S.; Hou, K.; Li, Z.; Wang, J. Graphene-based nanomaterials as lubricant additives: A review. *Lubricants* **2022**, *10*, 273. [CrossRef]
25. Bunch, J.S.; Verbridge, S.S.; Alden, J.S.; Van Der Zande, A.M.; Parpia, J.M.; Craighead, H.G.; McEuen, P.L. Impermeable Atomic Membranes from Graphene Sheets. *Nano Lett.* **2008**, *8*, 2458–2462. [CrossRef] [PubMed]
26. Wohlgemuth, M.; Mayer, M.; Rappen, M.; Schmidt, F.; Saure, R.; Grätz, S.; Borchardt, L. From Inert to Catalytically Active Milling Media: Galvanostatic Coating for Direct Mechanocatalysis. *Angew. Chem. Int. Ed.* **2022**, *61*, e202212694. [CrossRef] [PubMed]
27. Hsu, S.M.; Gates, R.S. Effect of materials on tribochemical reactions between hydrocarbons and surfaces. *J. Phys. D Appl. Phys.* **2006**, *39*, 3128–3137. [CrossRef]
28. Ta, T.D.; Tieu, A.K.; Tran, B.H. Influences of iron and iron oxides on ultra-thin carbon-based tribofilm lubrication. *Tribol. Int.* **2022**, *173*, 107665. [CrossRef]
29. Shirani, A.; Li, Y.; Eryilmaz, O.L.; Berman, D. Tribocatalytically-activated carbon-based triboilm formation for wear reduction in alkane environment. *Sci. Rep.* **2021**, *11*, 20643. [CrossRef]

30. Zheng, X.; Zhu, H.; Kosasih, B.; Tieu, A.K. A molecular dynamics simulation of boundary lubrication: The effect of n-alkanes chain length and normal load. *Wear* **2013**, *301*, 62–69. [CrossRef]
31. Vijayan, S.; Luo, N.; Aindow, M. Microstructural stability and phase transformations in electrodeposited cobalt-phosphorus coatings. *J. Alloys Compd.* **2017**, *719*, 142–150. [CrossRef]
32. Yang, B.; Qin, G.; Pei, W.; Ren, Y.; Xiao, N. Sputtered amorphous Co–Pt–P thin films for soft underlayer of perpendicular magnetic recording. *J. Magn. Magn. Mater.* **2010**, *322*, 1854–1858. [CrossRef]
33. Guo, Y.; Feng, Q.; Ma, J. The hydrogen generation from alkaline NaBH4 solution by using electroplated amorphous Co–Ni–P film catalysts. *Appl. Surf. Sci.* **2013**, *273*, 253–256. [CrossRef]
34. Gawande, M.B.; Goswami, A.; Felpin, F.-X.; Asefa, T.; Huang, X.; Silva, R.; Zou, X.; Zboril, R.; Varma, R.S. Cu and Cu-Based Nanoparticles: Synthesis and Applications in Catalysis. *Chem. Rev.* **2016**, *116*, 3722–3811. [CrossRef]
35. Knudsen, J.; Nilekar, A.U.; Vang, R.T.; Schnadt, J.; Kunkes, E.L.; Dumesic, J.A.; Mavrikakis, M.; Besenbacher, F. A Cu/Pt Near-Surface Alloy for Water−Gas Shift Catalysis. *J. Am. Chem. Soc.* **2007**, *129*, 6485–6490. [CrossRef] [PubMed]
36. Feng, Z.; Xiao, Y.-L.; Zhang, X. Transition-Metal (Cu, Pd, Ni)-Catalyzed Difluoroalkylation via Cross-Coupling with Difluoroalkyl Halides. *Accounts Chem. Res.* **2018**, *51*, 2264–2278. [CrossRef]
37. Takenaka, S.; Ogihara, H.; Yamanaka, I.; Otsuka, K. Decomposition of methane over supported-Ni catalysts: Effects of the supports on the catalytic lifetime. *Appl. Catal. A Gen.* **2001**, *217*, 101–110. [CrossRef]
38. Shirani, A.; Al Sulaimi, R.; Macknojia, A.Z.; Eskandari, M.; Berman, D. Tribocatalytically-active nickel/cobalt phosphorous films for universal protection in a hydrocarbon-rich environment. *Sci. Rep.* **2023**, *13*, 10914. [CrossRef]
39. Pingale, A.D.; Owhal, A.; Katarkar, A.S.; Belgamwar, S.U.; Rathore, J.S. Recent researches on Cu-Ni alloy matrix composites through electrodeposition and powder metallurgy methods: A review. *Mater. Today Proc.* **2021**, *47*, 3301–3308. [CrossRef]
40. Mahajan, C.; Hasannaeimi, V.; Pole, M.; Kautz, E.; Gwalani, B.; Mukherjee, S. Corrosion mechanisms in model binary metallic glass coatings on mild steel and correlation with electron work function. *Corros. Sci.* **2022**, *207*, 110578. [CrossRef]
41. Saidi, M.; Pasc, A.; El Moujahid, C.; Canilho, N.; Badawi, M.; Delgado-Sanchez, C.; Celzard, A.; Fierro, V.; Peignier, R.; Kouitat-Njiwa, R.; et al. Improved tribological properties, thermal and colloidal stability of poly-α-olefins based lubricants with hydrophobic MoS2 submicron additives. *J. Colloid Interface Sci.* **2020**, *562*, 91–101. [CrossRef]
42. Liu, Y.; DiFoggio, R.; Sanderlin, K.; Perez, L.; Zhao, J. Measurement of density and viscosity of dodecane and decane with a piezoelectric tuning fork over 298–448K and 0.1–137.9 MPa. *Sens. Actuators A Phys.* **2011**, *167*, 347–353. [CrossRef]
43. Zeegers-Huyskens, T.; Huyskens, P. Intermolecular forces. In *Intermolecular Forces: An Introduction to Modern Methods and Results*; Springer: Berlin/Heidelberg, Germany, 1991; pp. 1–30.
44. Morriss, G.P.; Daivis, P.J.; Evans, D.J. The rheology of *n* alkanes: Decane and eicosane. *J. Chem. Phys.* **1991**, *94*, 7420–7433. [CrossRef]
45. Patel, S.; Azad, A.; Khan, M. Numerical investigation for predicting diesel engine performance and emission using different fuels. *Energy Procedia* **2019**, *160*, 834–841. [CrossRef]
46. Yi, Y.; Xing, J.; Wan, M.; Yu, L.; Lu, Y.; Jian, Y. Effect of Cu on microstructure, crystallography and mechanical properties in Fe-B-C-Cu alloys. *Mater. Sci. Eng. A* **2017**, *708*, 274–284. [CrossRef]
47. Yi, Y.; Xing, J.; Lu, Y.; Gao, Y.; Fu, H.; Yu, L.; Wan, M.; Zheng, Q. Effect of normal load on two-body abrasive wear of an Fe-B-Cr-C based alloy with minor Cu and Ni additions. *Wear* **2018**, *408–409*, 160–170. [CrossRef]
48. Liu, H.; Xu, Q.; Wang, C.; Zhang, X. Corrosion and wear behavior of Ni_{60}CuMoW coatings fabricated by combination of laser cladding and mechanical vibration processing. *J. Alloys Compd.* **2015**, *621*, 357–363. [CrossRef]
49. Alanazi, N.M.; El-Sherik, A.; Alamar, S.H.; Shen, S. Influence of residual stresses on corrosion and wear behavior of electrodeposited nanocrystalline cobalt-phosphorus coatings. *Int. J. Electrochem. Sci.* **2013**, *8*, 10350–10358. [CrossRef]
50. Rochefort, A.; Vernisse, L.; Gómez-Herrero, A.C.; Sánchez-Sánchez, C.; Martín-Gago, J.A.; Chérioux, F.; Clair, S.; Coraux, J.; Martínez, J.I. Role of the Structure and Reactivity of Cu and Ag Surfaces in the Formation of a 2D Metal–Hexahydroxytriphenylene Network. *J. Phys. Chem. C* **2021**, *125*, 17333–17341. [CrossRef]
51. Sinfelt, J.; Carter, J.; Yates, D. Catalytic hydrogenolysis and dehydrogenation over copper-nickel alloys. *J. Catal.* **1972**, *24*, 283–296. [CrossRef]
52. Khan, A.M.; Ahmed, J.; Liu, S.; Martin, T.; Berkebile, S.; Chung, Y.-W.; Wang, Q.J. Formation of Wear-Protective Tribofilms on Different Steel Surfaces During Lubricated Sliding. *Tribol. Lett.* **2023**, *71*, 101089. [CrossRef]
53. Li, Z.; Deng, L.; Kinloch, I.A.; Young, R.J. Raman spectroscopy of carbon materials and their composites: Graphene, nanotubes and fibres. *Prog. Mater. Sci.* **2023**, *135*, 101089. [CrossRef]